Mapping C–HxxxM Interactions in Confined Spaces: (a-ICyD Me)Au, Ag, Cu Complexes Reveal "Contra-electrostatic H-bonds" Masquerading as Anagostic Interactions

Gabriel dos Passos Gomes, Guangcan Xu, Xiaolei Zhu, Lise-Marie Chamoreau, Yongmin Zhang, Olivia Bistri-Aslanoff, Sylvain Roland, Igor Alabugin, Matthieu Sollogoub

Mapping C–H···M Interactions in Confined Spaces: (α-ICyD^{Me})Au, Ag, Cu Complexes Reveal "Contra-electrostatic H-bonds" Masquerading as Anagostic Interactions

Dr. Gabriel dos Passos Gomes,[1,3] Dr. Guangcan Xu,[2] Dr. Xiaolei Zhu,[2] Dr. Lise-Marie Chamoreau,[2] Dr. Yongmin Zhang,[2] Dr. Olivia Bistri-Aslanoff,[2] Dr. Sylvain Roland,[2] Prof. Igor V. Alabugin,*[1] Prof. Matthieu Sollogoub*[2]

[1]: Department of Chemistry and Biochemistry, Florida State University, Tallahassee, FL, USA, 32309
[2]: Sorbonne Université, CNRS, Institut Parisien de Chimie Moléculaire, UMR 8232, 4 place Jussieu, 75005 Paris, France
[3]: *Current address*: Department of Chemistry and Department of Computer Science, University of Toronto, Toronto, ON, Canada, M5S 3H6
*: corresponding authors alabugin@chem.fsu.edu, matthieu.sollogoub@sorbonne-universite.fr
Twitter : @IAlabugin, @SollogoubM

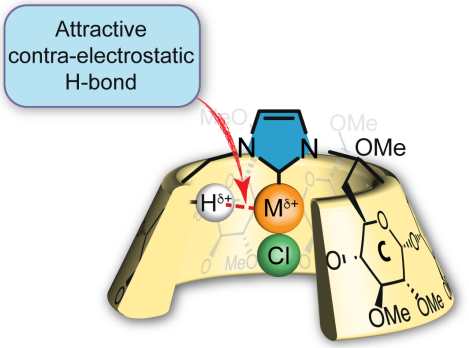

(α-ICyD^{Me})MCl, M= Ag, Cu, Au

What happens when a C–H bond is forced to interact with unpaired pairs of electrons at a positively charged metal? Such interactions can be considered as "contra-electrostatic" H-bonds, which combine the familiar orbital interaction pattern characteristic for the covalent contribution to the conventional H-bonding with an unusual contra-electrostatic component. Such remarkable C–H···M attractive interaction became experimentally accessible within (α-ICyD^{Me})MCl, NHC–Metal complexes embedded into cyclodextrins.

Abstract: What happens when a C–H bond is forced to interact with unpaired pairs of electrons at a positively charged metal? Such interactions can be considered as "contra-electrostatic" H-bonds, which combine the familiar orbital interaction pattern characteristic for the covalent contribution to the conventional H-bonding with an unusual contra-electrostatic component. While electrostatics is strongly stabilizing component in the conventional C–H···X bonds where X is an electronegative main group element, it is destabilizing in the C–H···M contacts when M is Au(I), Ag(I), or Cu(I) of NHC–M–Cl systems. Such remarkable C–H···M interaction became experimentally accessible within (α-ICyD^{Me})MCl, NHC–Metal complexes embedded into cyclodextrins. Computational analysis of the model systems suggests that the overall interaction energies are relatively insensitive to moderate variations in the directionality of interaction between a C–H bond and the metal center, indicating stereoelectronic promiscuity of fully filled set of *d*-orbitals. A combination of experimental and computational data demonstrates that metal encapsulation inside the cyclodextrin cavity forces the C–H

bond to point toward the metal, and reveals a still attractive "contra-electrostatic" H-bonding interaction.

Keywords: Confinement, C-H metal interactions, anagostic interactions, H-bonds, cyclodextrins, coinage metals, NHC

Introduction

The alkane C–H bonds are poorly suited for coordination to a metal center. Because these non-polar, weakly polarizable, strong bonds are associated with a low energy orbitals $\sigma_{CH,}$ and the high-energy orbitals σ^*_{CH} the alkane C–H bonds are neither effective donors nor strong acceptors. Nevertheless, alkane-metal complexes exist, and interactions of C–H bonds with metal centers are interesting for many reasons, both fundamental and applied.[1-4]

Interest in such interactions was catalyzed by the discovery of the strong "agostic" C–H···M interactions, which possess a significant degree of *three-center, two-electron* (*3c,2e*)-character, and observed for the strongly electron-deficient metal centers.[5-8] Such complexes can play a role as intermediates in C–H activation.[9-13] Subsequently, a variety of weaker "anagostic" C–H···M interactions were identified.[14-16] This term stands for a broad selection of interactions that can be repulsive or attractive,[17] purely electrostatic, or partially covalent.[18] The common point to all these interactions is that they are not agostic; hence anagostic interactions stand for something else than agostic.[19,20]

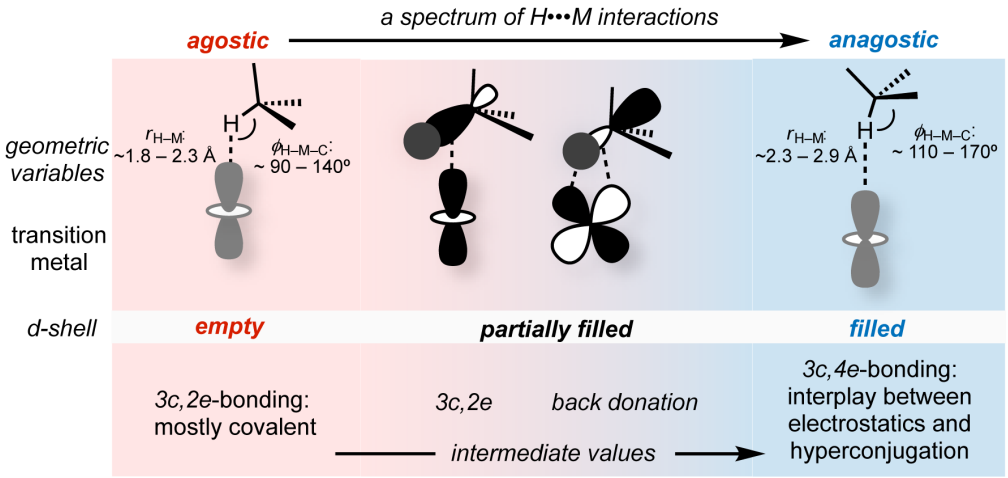

Scheme 1. The spectrum of C–H···metal interactions.

The nature of the interaction depends strongly on the metal and its electron population. The agostic and anagostic interactions have been well-studied for d^8 metal complexes (Scheme 1), but "anagostic" interactions were also invoked for the low oxidation state metal complexes with at least partially filled *d*-shell (*e.g.*, d^6, d^8, d^{10}).[1,21] For the M(I) complexes with M = Au, Ag, Cu, all *d*-orbitals are filled, precluding strong agostic interactions and leaving anagostic interactions as the main choice.[22] The question of Au···H interactions has fascinated many, and the Au···H-C H-bonding has been

discussed and proposed.[23-27] However, the exact nature of the interaction is still under debate, and only recently, a genuine H-bonding was evidenced but for the strongly polarized N-H bond in an R_3N^+-H···Au complex,[28] or for interactions between water and the $AuMe_2$-anion.[29]

Since the coinage metals often act as Lewis acids, orbital perturbations, and polarization induced by electrostatic interactions should influence their reactivity. The spectroscopic signatures of which interactions have been used to get deeper insights into their electronic origin.[18,30-32] Recently, the Sollogoub group reported synthesis,[33] NMR analysis,[34] and catalytic applications[33-37] of several NHC–MX complexes with M = Au, Ag, Cu embedded in a cyclodextrin cavity (Figure 1).[38] These well-defined NHC–capped cyclodextrins (ICyDs) are characterized by a network of introverted cavity protons, which show intriguing behavior by ^{1}H NMR spectroscopy. For instance, a comparison of the unmetalated imidazolium compounds with the corresponding metal complexes showed that H^5 protons, which are pointing toward the inside of the cavity near the primary rim of the cyclodextrin, undergo a strong deshielding, which depends on the nature of the metal (Figure 1). These cyclodextrins could not be crystallized to obtain a 3D structure, probably because they are *O*-benzylated. However, we were able to model their structure and show that H^5 were close to the metal. Furthermore, the most deshielded protons were also the closest to the metal. Therefore, we attributed this deshielding to a C–H···M interaction. Upon examination of the model, we found that the closest H^5 was situated at *ca.* 2.5 Å from the metal with a C–H^5-M angle of 145°, which, together with deshielding, was reported to be diagnostic of an anagostic interaction. However, conventional hydrogen bonding to the halogen of M-X moiety could have similar effects. So, in order to understand the nature of anagostic interactions at play and to get insight into the reactivity of these complexes from an electronic viewpoint, it was necessary to go deeper into the electronic analysis of these systems. In combination with structural details obtained from crystal structures, electronic structure analyses offer a unique opportunity for understanding the details of C–H interactions with the NHC complexes of the coinage metals as a function of geometrical parameters, such as H···M distance and C–H···M angle, as well as the nature of metal.

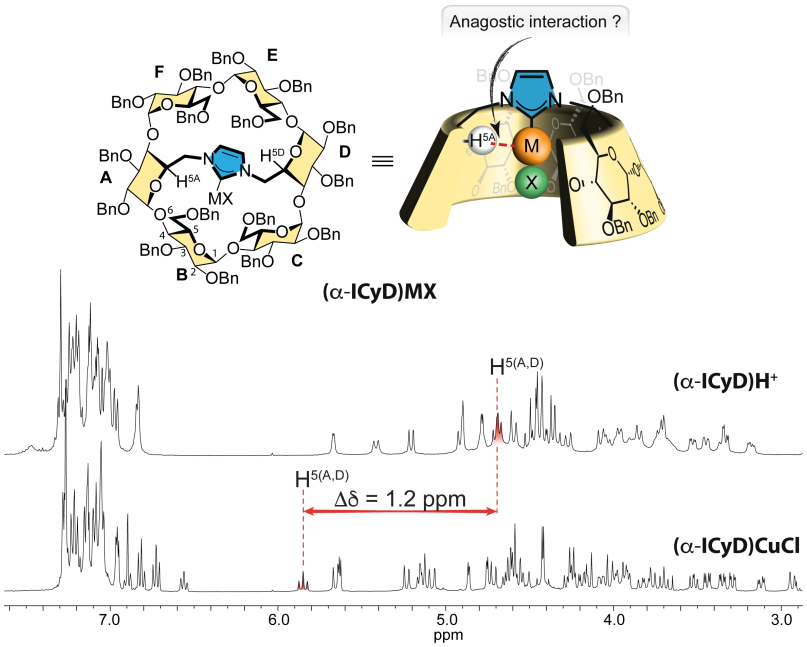

Figure 1. Structure of (α-ICyD)MX and numbering of sugar carbons (1 to 6) and of glucose units on the cyclodextrin (A to F) (top left). 3D representation of (α-ICyD)MX showing the MX complex embedded in a cyclodextrin cavity where H^{5A} interacts with M (top right). ^{1}H NMR of imidazolium (α-ICyD)H^{+} (top) and (α-ICyD)CuCl (bottom) showing the characteristic deshielding of $H^{5(A,D)}$

In the present work, we spectroscopically studied the *O*-methylated ($ICyD^{Me}$) version of the *O*-benzylated ICyDs, and obtained X-ray crystal structures showcasing the C–H···M interactions in their cavity. We then computationally probed the response of C–H bond lengths to the proximity and orientation of the C–H bond relative to the metal center. We started by analyzing the parent CH_4···metal complexes and then showed how the general trends for the C–H···M interactions are transferred to the C–H bonds in the cyclodextrin cavities. In order to understand the nature of C–H···metal interactions, we investigated the orbital interactions involved in these contacts using Natural Bond Orbital (NBO) and Natural Energy Decomposition analyses (NEDA). An unusual feature of these coinage M···H-C interactions is that even though the metal center has non-bonding doubly occupied orbitals (*i.e.*, the *d*-type lone pairs, *vide infra*) and can serve as a Lewis base, it also bears a significant partial positive charge. Hence, although the anagostic M···H-C interactions with such "cationic Lewis bases" share the familiar *3c,4e*-features with conventional hydrogen bonds, their electrostatic interaction with a typical H-bond donor should be drastically different. In the final part, we explore how the experimentally observed trends in the rigid X-ray geometries correspond to the anisotropic response observed for the C–H bond in computed geometries. In the present system, metal encapsulation inside the cyclodextrin cavity forces the C–H bond to point toward the metal and forms the C–H···M contacts that can be considered as H-bonds that have an unusual "contra-electrostatic" component but still potentially attractive (Scheme 2).

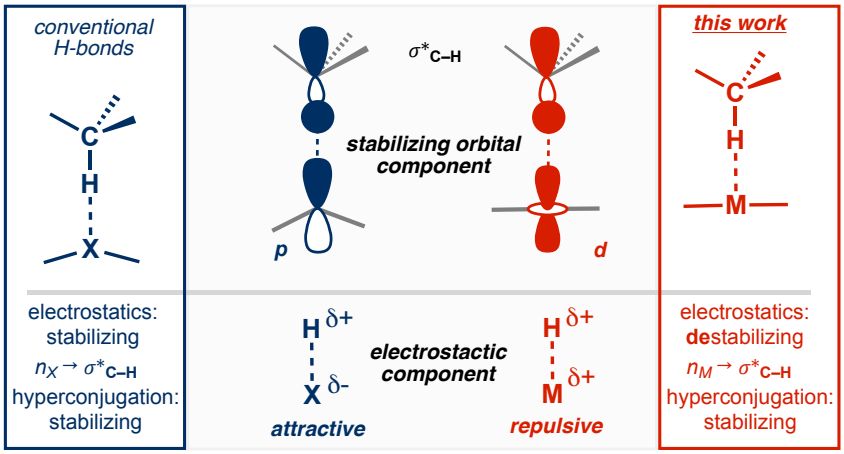

Scheme 2. Comparison of orbital and electrostatic contributions to C–H···M interactions and conventional H-bonds

Results and Discussion

Experimental analysis

A prerequisite for a detailed study of the electronic effects involving the coinage metal encapsulated in the cyclodextrin cavity of an ICyD ligand is to get a crystal structure. We have shown that the replacement of benzyl groups with methyls on ICyD ligands could lead to the crystallization of (α-ICyD^{Me})AgCl.[39] We also previously synthesized (α-ICyD^{Me})CuCl, (α-ICyD^{Me})AgCl, and (α-ICyD^{Me})AuCl and characterized them by NMR. They all displayed deshieldings of H^5 characteristic of the metal complex confined inside the cyclodextrin cavity. More precisely, in the three complexes, $H^{5(A,D)}$ were the most deshielded (5.55–6.32 ppm). The gold complex displayed the strongest deshielding for this pair of H^5 (6.32 ppm) but also showed stronger deshieldings than silver and copper complexes for all other H^5 (Figure 2, Table1). (α-ICyD^{Me})CuCl, and (α-ICyD^{Me})AuCl crystals could now be obtained through slow diffusion of pentane and cyclohexane into a solution of the complex in $CDCl_3$. Interestingly, though the (α-ICyD^{Me})AgCl, (α-ICyD^{Me})CuCl X-ray structures are C_2-symmetrical and quasi isomorphous, the structure of (α-ICyD^{Me})AuCl is not. This dissonance seems to be due to a different packing in the solid-state. In solution, however, this phenomenon does not occur, and the three compounds are C_2-symmetrical in the NMR. Adding the hydrogen atoms to the heavy atoms in these structures, we determined M···H^5 distances as well as C–H^5-M, H^5-M-Cl angles, and N-C-M-H^5 dihedral angles (Table 2). All distances are in the same range, although slightly longer on average for Au, and the closest protons from the metal are also the most deshielded in the NMR.

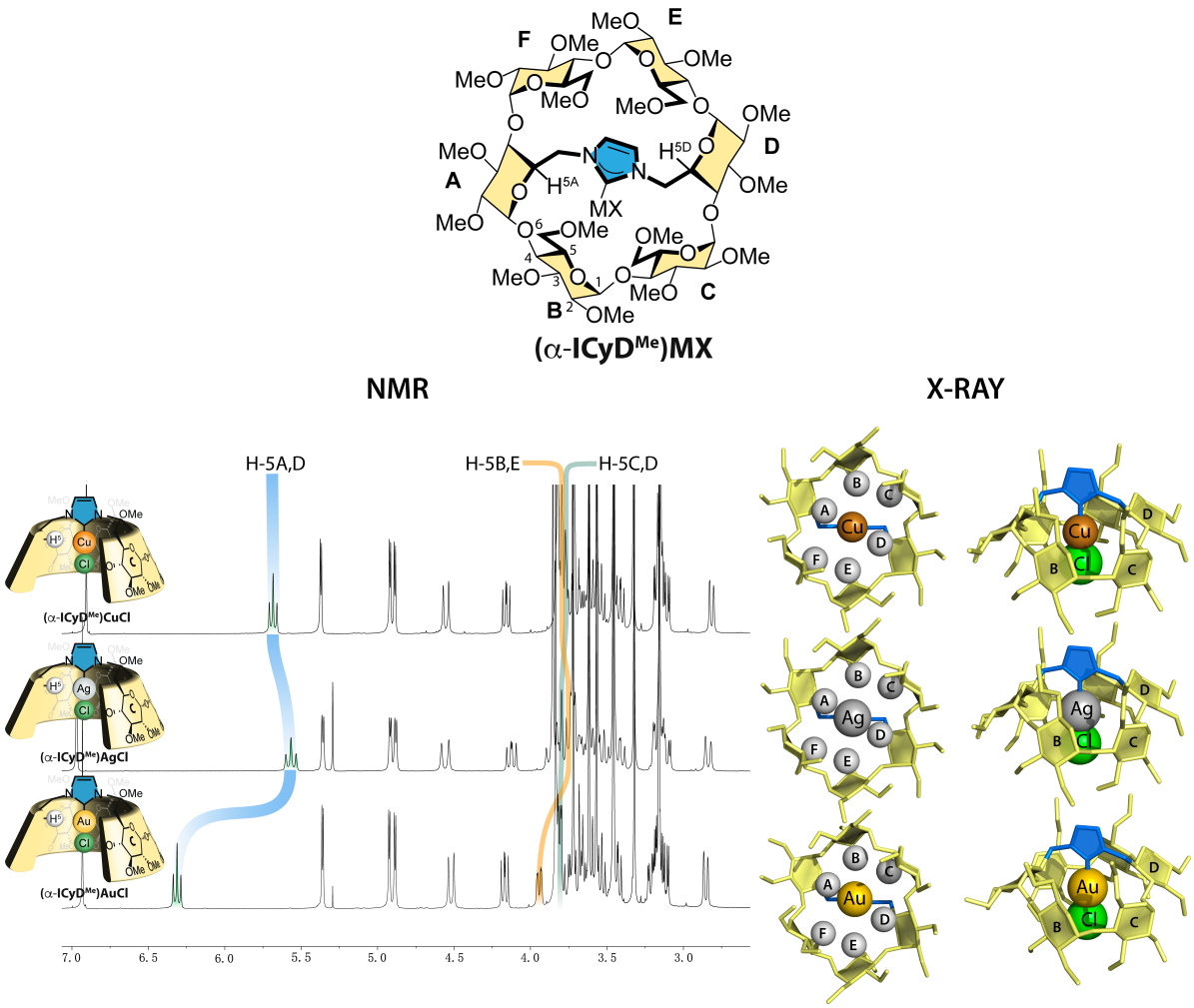

Figure 2. Left: ^{1}H NMR spectra of (α-ICyD^{Me})CuCl, (α-ICyD^{Me})AgCl and (α-ICyD^{Me})AuCl (400 MHz, $CDCl_3$)[39]; Right: X-ray crystal structure of (α-ICyD^{Me})CuCl, (α-ICyD^{Me})AgCl and (α-ICyD^{Me})AuCl from $CDCl_3$/pentane/cyclohexane H^5s are shown as pale grey spheres.

Table 1. Experimental ^{1}H chemical shifts of the H^5s (400 MHz, $CDCl_3$)[39]

Compound	$H^{5(A,D)}$	$H^{5(B.E)}$	$H^{5(C,F)}$
(ICyD^{Me})CuCl	5.67	3.77	3.75
(ICyD^{Me})AgCl	5.55	3.68	3.72
(ICyD^{Me})AuCl	6.32	3.96	3.83

Table 2. Distances and angles from X-ray crystal structures (Hydrogen atoms were placed at calculated positions in the model)[39]

	d_{M-H^5} (Å)	C–H⁵–M angle	H⁵-M-Cl angle	H⁵–M–C–N dihedral	d_{M-H^5} (Å)	C–H⁵–M angle	H⁵–M–Cl angle	H⁵–M–C–N dihedral	d_{M-H^5} (Å)	C–H⁵–M angle	H⁵–M–Cl angle	H⁵–M–C–N dihedral
	H$^{5(A,D)}$				**H$^{5(B.E)}$**				**H$^{5(C,F)}$**			
(ICyD^{Me})CuCl	2.5	140	104	154	3.3	150	99	87	3.8	153	99	43
	H$^{5(A,D)}$				**H$^{5(B.E)}$**				**H$^{5(C,F)}$**			
(ICyD^{Me})AgCl	2.5	143	109	154	3.3	152	102	87	3.9	149	102	44
	H^{5A}				**H^{5B}**				**H^{5C}**			
(ICyD^{Me})AuCl	2.7	134	110	151	3.7	158	109	93	3.9	152	105	49
	H^{5D}				**H^{5E}**				**H^{5F}**			
	2.5	142	102	-21	3.3	159	99	-84	3.4	156	101	-135

Computational Analysis

With the NMR analysis and the crystal structure of all three (α-ICyD^{Me})MCl complexes in hand, we started the computational study with a brief survey of the electronic structure of the NHC–Au-Cl system. The LUMO is at the NHC ligand with little contribution from the metal. On the other hand, the HOMO is an antibonding combination of one of the Au-*d*-orbitals with a lone pair of Cl. Since the metal center contributes more to the HOMO than to the LUMO, one can expect that the metal center will be mostly a donor partner in the donor-acceptor interactions. However, one has to bear in mind that the Au(I) also has a considerable positive charge (+0.37 *e*, from the Natural Population Analysis). The effect of this positive charge is reflected in the relatively low energy of the Au *d*-orbitals (HOMO-4 and below) (Scheme 3).

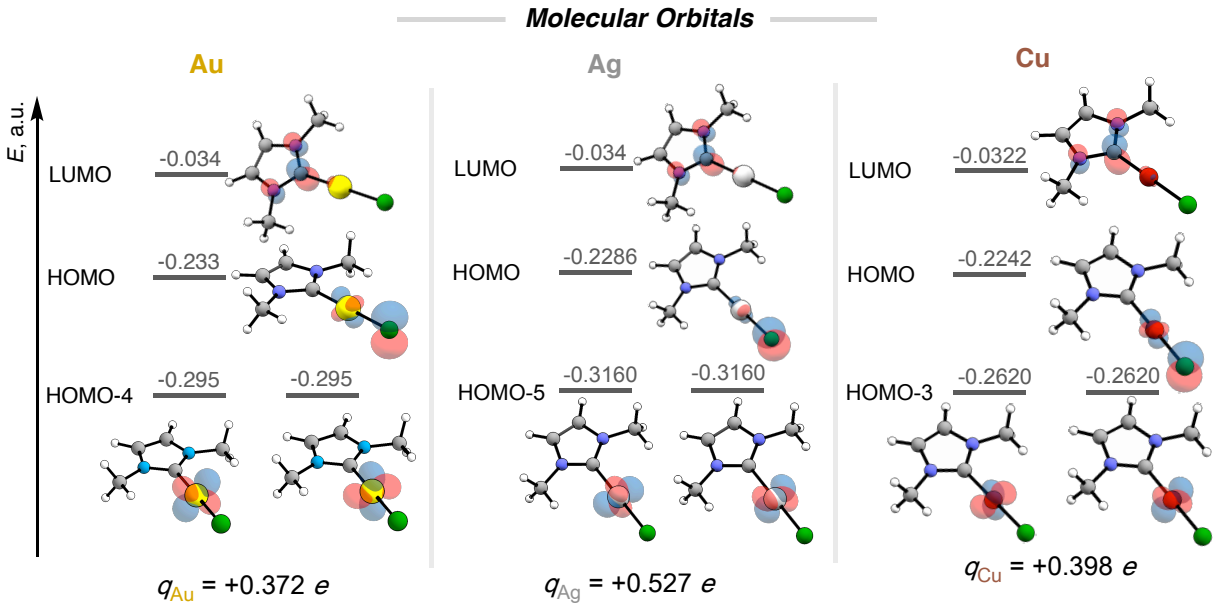

Scheme 3. The molecular orbitals for the investigated NHC–M-Cl systems (M=Au, Ag, Cu).

The observation that the HOMO and the LUMO are located at the opposite parts of the molecule suggests that the donor-acceptor interactions of the C–H moiety with such metal complexes are likely to be quite anisotropic; *i.e.*, their nature may strongly depend

on the exact position of the C–H bond relative to the ligands. This analysis was also performed for the Ag and Cu complexes, with similar trends observed. The LUMO energies are virtually identical since this orbital is mostly concentrated on the NHC moiety. Although the HOMO energies differ only slightly since the contribution of the metal to this MO is relatively low, the order of the HOMO energies (Au<Ag<Cu) does agree with the relative electronegativities of these elements.
Interestingly, the atomic charges at the three metal centers (Ag>Cu>Au) do not follow the above trend as the HOMO energies. Furthermore, the energy of lower energy occupied MOs corresponding closely to *d*-orbitals at the metal center increases in the following order Ag<Au<Cu (Scheme 3). These observations suggest that the interaction between the metal and the ligand are complex and involve more than one component.

Methane complexes as probes for C–H···M interactions

Because the fundamental understanding for the interaction of C–H bonds with the NHC–MX systems is still lacking, we started this investigation by using methane, the simplest hydrocarbon with an sp^3 C–H bond. The symmetry of this molecule, as well as the absence of other functional groups that can interact with the metal complex considerably, simplifies the electronic situation, allowing one to concentrate on the intrinsic effects associated with the C–H···Metal interaction.
So, how does the C–H bond interact with the metal center? And how does this interaction respond to changes in distance and orientation of the two interacting partners? We have considered three geometric parameters illustrated in the scheme below: a) the H···M distance, b) the H–M–Cl angle, and c) the H–M–C1–N dihedral (Scheme 4A). The changes of electronic structure, geometry, and stability of the complexes as a function of these three parameters are illustrated in this section.

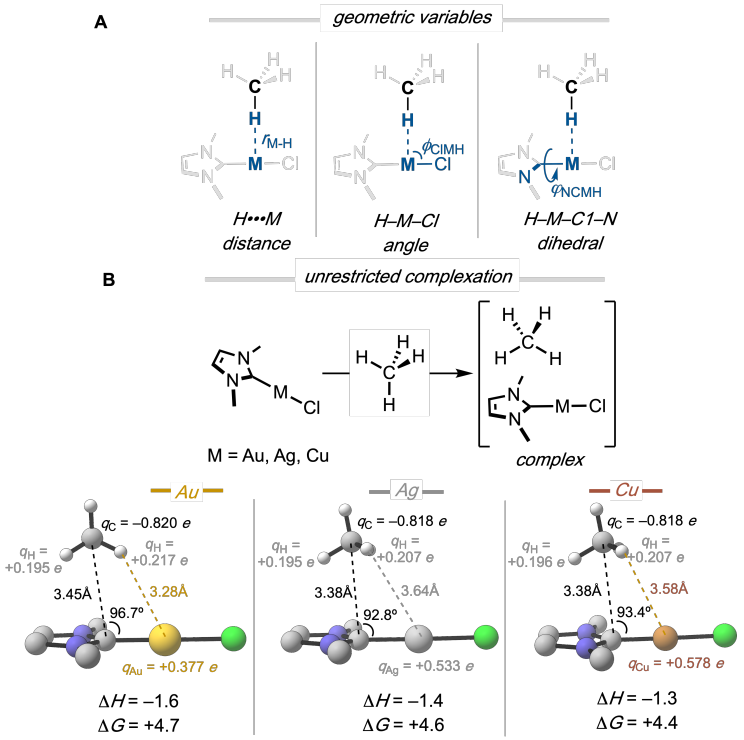

Scheme 4. A: The three geometric variables used for charting the supramolecular space for the C–H···M interactions between methane and the NHC–M-Cl complexes. **B**: Unrestricted optimized geometries for the three complexes. Energies in kcal/mol.

We have also located the energy minima corresponding to the complexes. All three complexes have a negative enthalpy of formation (*ca.* 1.5 kcal/mol), indicating that these intermolecular interactions are attractive (Scheme 4B). Because the attraction is relatively weak, the entropic penalty for the formation for bringing two components together renders the Gibbs energy positive (*ca.* +4.5 kcal/mol). For the unstrained complexes, other electrostatic components contribute as well to the observed geometries. Of course, neither this entropic penalty will apply to our cyclodextrin systems where such interactions are *intra*molecular, nor the calculated geometric preference for the complexes be preserved on these shallow energy surfaces because the cyclodextrin systems impose their own geometric restrictions on the position of the carbohydrate C–H bonds. We can use geometric constraints (Scheme 4A) to explore the structural and spectroscopic consequences of C–H···M contacts away from their intrinsic equilibrium geometries.

The H···M distance:

The effect of H···M distance was probed using a symmetric trajectory where both the C–H–M angle and the H–M–C1–N dihedral were constrained to 180 and 90 degrees, respectively. All other geometric parameters were allowed to change freely in the geometry optimizations. Under these constraints, the lowest energy was observed at the H···M distance of *ca.* 2.9 Å. The binding interaction was weak, as illustrated by minimal changes in energy at the greater H···M separations. Bringing the two interacting molecules closer led to progressive energy increase. This increase was initially small (~1 kcal/mol for the first 0.5 Å but exceeds 5 kcal/mol at distances shorter than 2.1 Å, where direct orbital interactions start to operate (Figure 3).

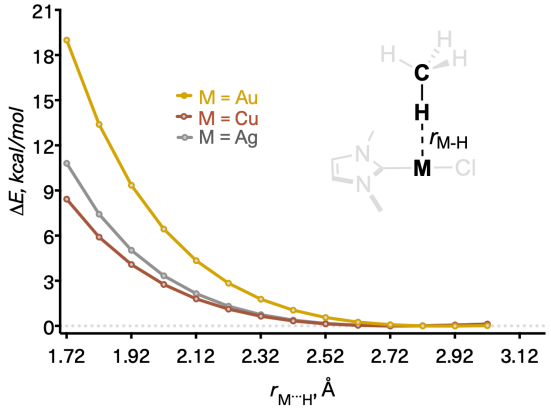

Figure 3. Relative energies for the CH_4···M (M = Au, Ag, Cu) distances. For Ag and Cu, the repulsive part of the distance scan starts at the shorter H···M distances.

The experimentally observed C–H···M distances (≥ 2.5 Å) correspond to the region where the interaction energies are quite small. Interestingly, computations suggest that the penalty for CH···M distance shortening is more significant for M=Au. This prediction is in

good agreement with the slightly larger CH···M experimental distances for the Au-complex in comparison to the Cu- and Ag-complexes (Table 2). The absence of a well-defined energy minimum characteristic for conventional H-bonds (where the H-bond acceptor is an electronegative heteroatom) is consistent with the unfavorable electrostatic forces in the C–H···M systems. In the latter case, both H and M have partial positive charges. With the electrostatic component opposite to that of the "normal" H-bonding, it is not surprising that, under these optimization constraints, the potential energy curve is not attractive.

The calculated C–H distance response to bringing the metal complex closer is small for the experimentally attainable H···M distances. Interestingly, the effect is larger for the Au-complex. The C–H bond starts to elongate as the H···M distance becomes shorter (Figure 4). This behavior is different from the more conventional C–H···Y H-bonding, where Y is a heteroatom with a lone pair. In the conventional cases, C–H bond contraction (blue-shifted H-bonds) is often observed first, followed by C–H bond elongation at the shorter H···Y distances.[42]

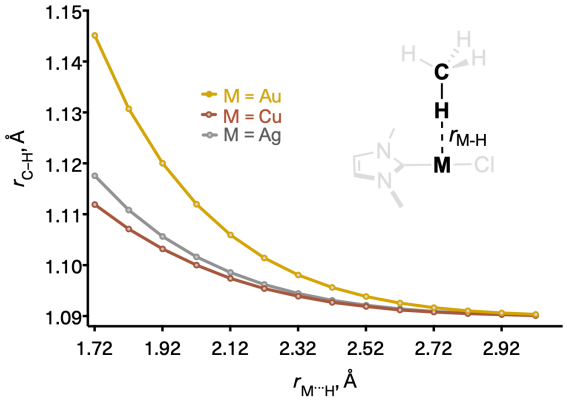

Figure 4. Effect of the M···H distance at the C–H bond length.

Evaluation of the total charge transfer revealed a surprising difference between the Au vs. Cu and Ag complexes. At the longer M···H distances, the methane molecule is a donor in all three complexes. However, at the distances of ~2.5-2.7 Å, methane behaves as *the net acceptor* in the Au complex but remains a donor in the Cu, Ag complexes. *The net donor ability of the Au-complex is observed even though the Au atom has a charge of +0.3 e*! Further compression of the M···H distance leads to an increase in the positive charge at the Cu and Ag complexes as well but at much shorter distances. (Figure 5)

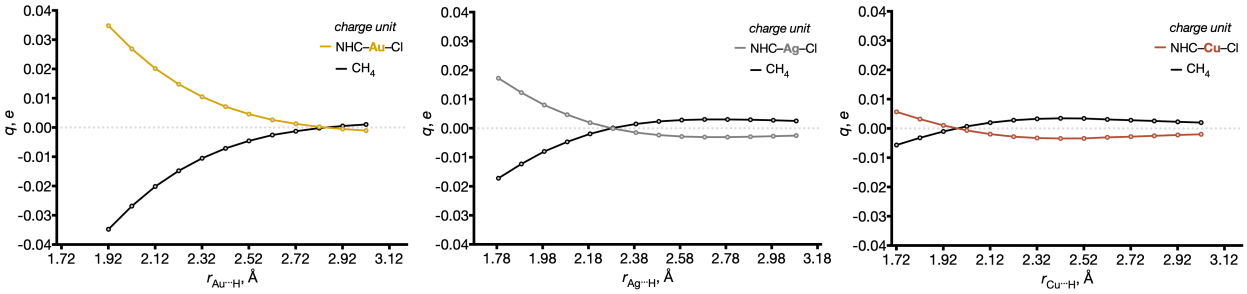

Figure 5. Effect of the M···H distance at the total natural charges of methane and NHC–M-Cl.

The carbon atom also loses electron density, and the intrinsic polarization of the C–H bond changes as hydrogen becomes less positively charged and gains electron density. Overall, hydrogen of the C–H bond becomes less positive as it gets closer to the metal. On the other hand, the carbon atom loses electron density. (Figures 6 and 7) This behavior is the opposite of the conventional C–H···Y bonding to a heteroatom. For example, hydrogen becomes more positively charged whereas carbon gains electron density as the H atom approaches the oxygen atom of water in the $F_3C–H···OH_2$ system.[42]

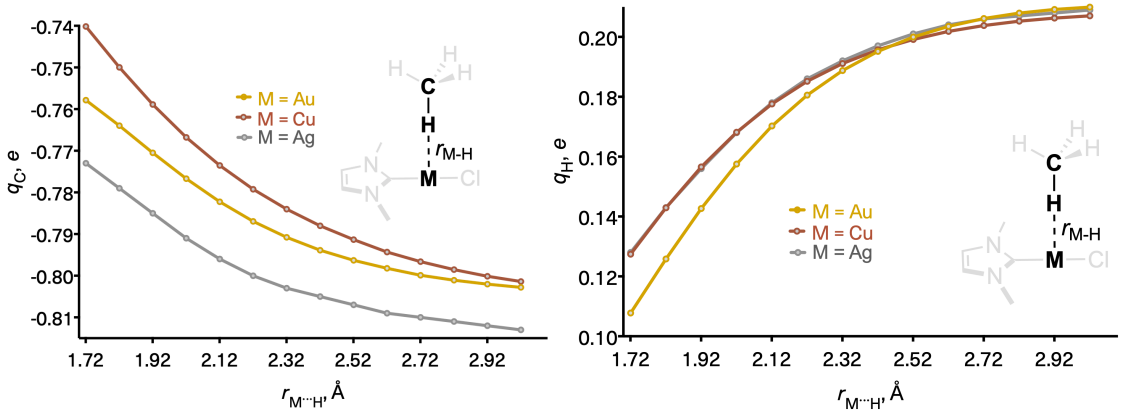

Figure 6. Effect of the M···H distance at the natural charges of methane's C and H specifically.

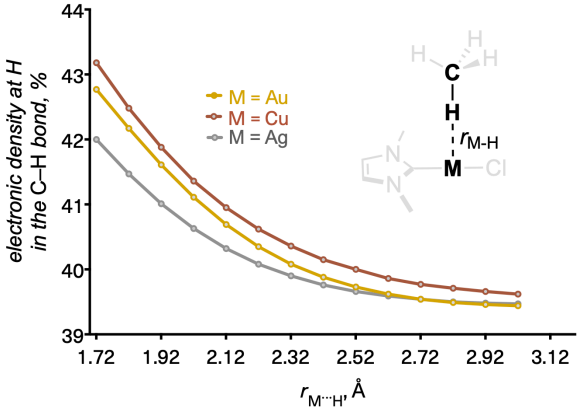

Figure 7. Polarization of the C–H bond (% electronic density at H) as a function of the M···H distance.

Analysis of the hybridization of the C–H bond provides an interesting insight into the nature of the electronic reorganization in this system. Initially, at the distances greater than 2.3 Å, the carbon hybrid of the interacting C–H bond gets additional *s*-character. This rehybridization[40,41] is similar to that observed at the early stages of the formation of blue-shifted H-bonds.[42] At the shorter distances, however, the carbon orbital gains *p*-character. This part of the curve for the C–H···M complexes is very different from what is observed for conventional H-bonding to electronegative heteroatoms where *s*-character at the C–H bond carbon hybrid continues to increase at the shorter distances. These differences are associated with the aforementioned opposite trends in the C–H bond repolarization in the two types of complexes (Figure 8).

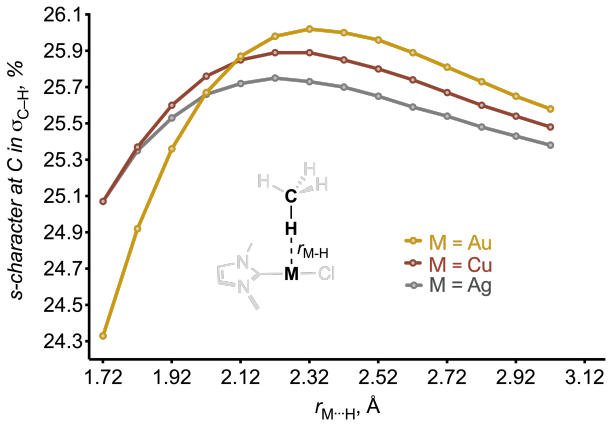

Figure 8. *s*-character at C in the C–H bond (%) as a function of the M–H distance.

We have also calculated the NBO changes in the population of the σ_{CH} and σ^*_{CH} orbitals in order to deeper understand the effects of the electronic origin of C–H bond elongation. A priori, one can attribute the observed C–H bond elongation (that should correspond to a red shifting of the IR-stretching frequencies) to one of the two effects: a) increased donations from the Au-moiety to the C–H bond at smaller distances (*i.e.*, the increased population of the antibonding σ^*_{CH} orbital) or b) donation from the C–H bond to the empty orbitals at gold (*i.e.*, the decreased population of the bonding σ_{CH} orbital). As the Au···H distance shortens, the bonding orbital is depleted of electron density whereas the antibonding orbital gains electron density. Both changes indicate a decrease in the C–H covalency. The more significant change in the σ^*_{CH} population (0.08 *e*) relative to the σ_{CH} population (0.03 *e*) suggests that the C–H bond is a net acceptor. Interestingly, the positively charged Au center, which is commonly used as a Lewis-acidic catalyst in organic reactions[33,34,43-52] serves as a donor in this particular situation. Again, the Au-complex is a better donor than its Ag and Cu counterparts (Figure 9).

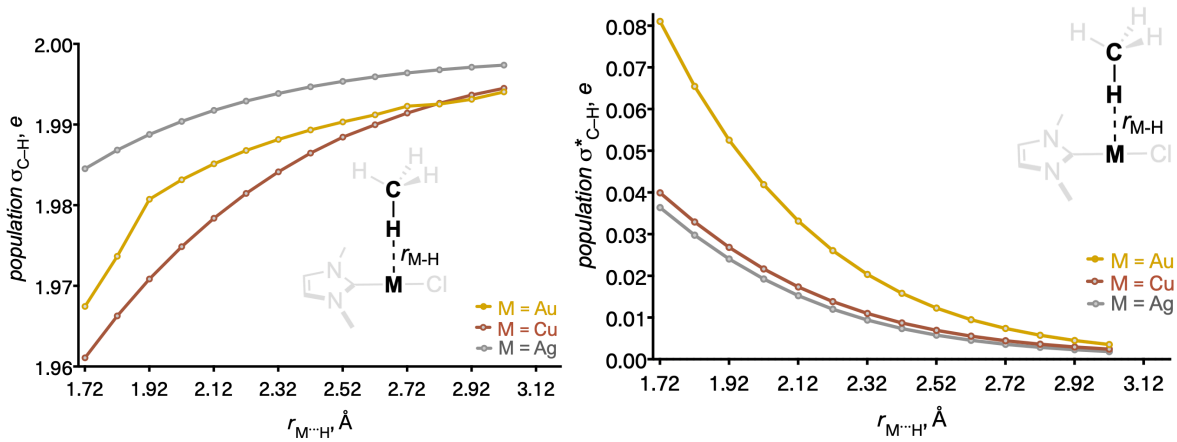

Figure 9. Electronic population of σ_{CH} (left) and σ^*_{CH} (right), both as a function of the M–H distances

The approach angle:

The Cl-M-H angle was scanned with the M-H distance fixed at 2.42 Å. The observed changes are smaller but still chemically significant. The stereoelectronic component is illustrated by the increase in energy when the angle deviates from the 80-115 range. The energy curve is nearly symmetric for the movement to NHC *vs.* Cl termini. At these C–H bond lengths (2.4 Å), the optimum H–M–Cl angle is ~95 degrees. The penalty for small deviations from this angle is not large – the scope of geometries in the range of 75-115 degrees are separated by less than 1 kcal/mol in terms of stability. Despite the minimal changes in energy, the C–H length shows a relatively complex behavior. The C–H distance curve is clearly less symmetric than the energy curve. Whereas methane tilting towards the NHC moiety (angles of >90 degrees) leads to C–H elongation, the opposite displacement (*i.e.*, tilting towards Cl) initially leads to the C–H bond contraction followed by C–H elongation at the strongly acute H–M–Cl angles (<70 degrees). An interesting observation is that, although the shapes of the C–H distance vs. Cl-M-H angle are similar for the three metals, the C–H bonds lengths for identical angles are different: Au>Ag>Cu (Figure 10).

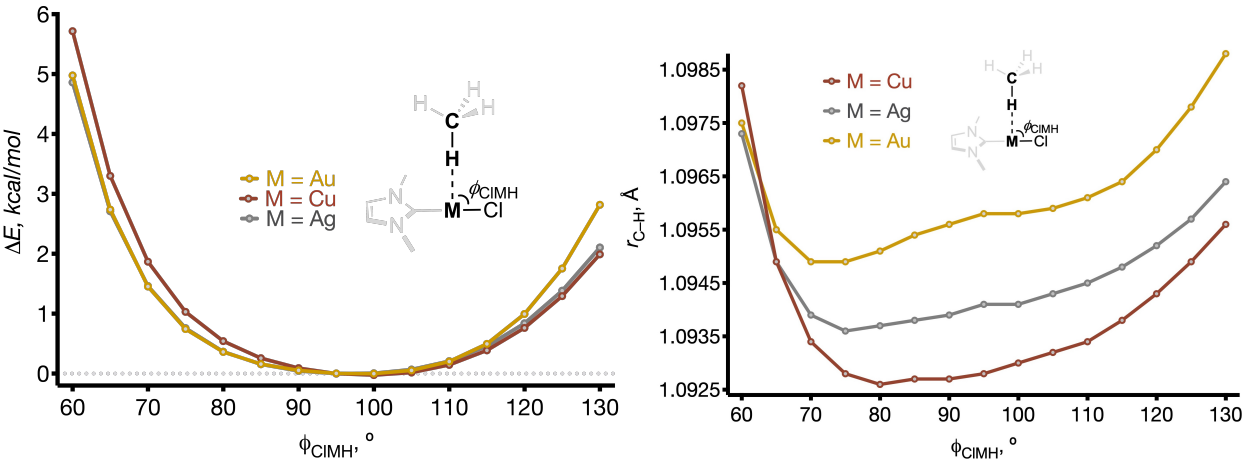

Figure 10. Left: relative energies for the Cl-M-H angle scans. Right: effect of the Cl-M-H angle at the C–H bond length. (M = Au, Ag, Cu).

The dihedral angle – *stereoelectronic promiscuity* of *d*-orbitals:
Scanning the N–C–M–H dihedral was performed for the M–H distance fixed at 2.42 Å, and the Cl-M-H angle fixed at 90°. The surface is very shallow — changes in both the energy and the C–H bond length in the region of 45–135 degrees are small. Only at the regions where C–H bonds get close to the sigma framework of the NHC–M complex, moderate destabilizing effects on energy and structure of the CH_4 molecule are observed (Figure 11).

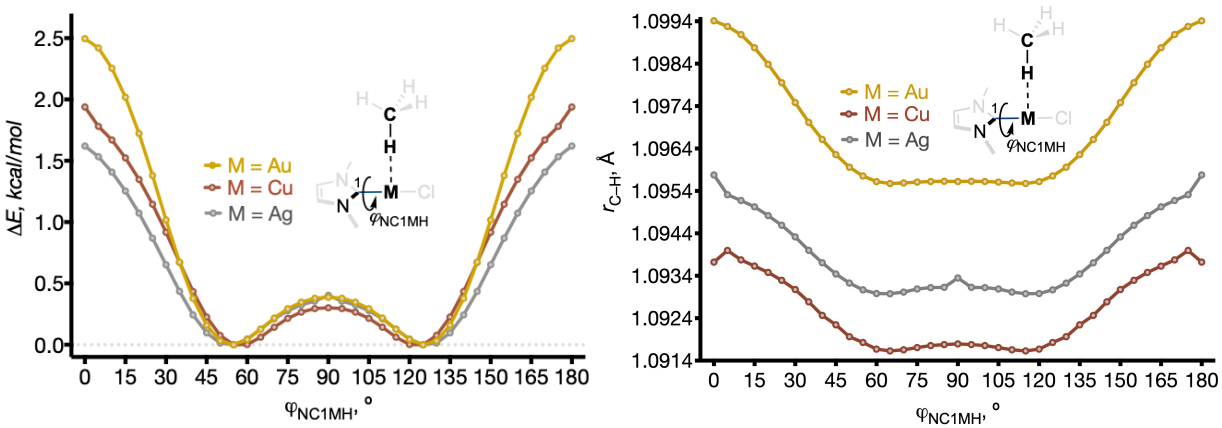

Figure 11. Left: relative energies for the N-C[1]-M-H dihedral angle scans. Right: effect of the N-C1-M-H dihedral angle at the C–H bond length. (M = Au, Ag, Cu).

Again, despite the similar overall shapes of the C–H distance vs. torsional angle, the C–H bond lengths for identical angles are different: Au>Ag>Cu. Furthermore, the C–H bonds in the vicinity of Au are slightly elongated relative to similar complexes with the Ag and Cu ions.

The reasons for the relatively low sensitivity to the torsional scan for each of the metals are stereoelectronic. The metal center has a manifold of *d*-orbitals of similar symmetry, which can serve as interaction partners for the C–H bond at a variety of dihedral angles. These orbitals are shown in Figure 12. As the C–H bond explores a new region of space by moving around the metal, it starts to engage in a new favorable orbital interaction as an old interaction gets weakened.

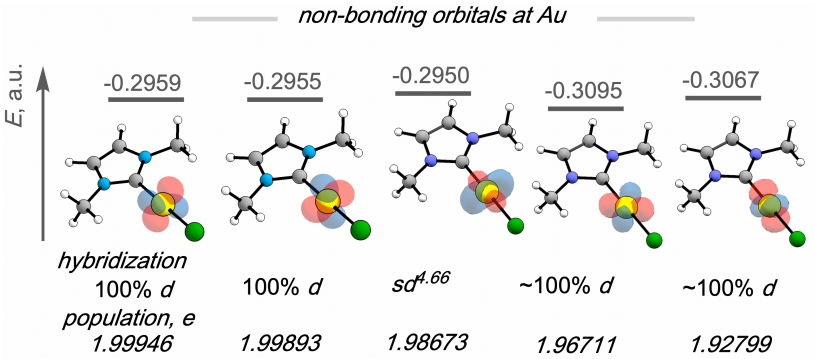

Figure 12. Hybridization, population, and energy level of gold's non-bonding orbitals in NHC–Au-Cl.

Comparison with the conventional H-bonds:
At this point, let us summarize the key trends of this study. DFT computations reveal that the C–H bond elongates as the H···M distances shorten. From the electronic point of view, shortening of H···M distances results in a decrease of the charge on H and an increase on C together with a net donation of the metal into the σ^*_{CH}. The penalty for small deviations from the perpendicular approach is not large — the range of geometries in the range of 75-115 degrees are separated by less than 1 kcal/mol in stability. Changes caused by reorientation of the C–H bond relative to the molecular plane of the complex, *i.e.*, the variations in the NC[1](carbene)–M–H dihedral angle are also minor due to "*stereoelectronic promiscuity*" of the fully filled metal *d*-orbital manifold. As the C–H bond rotates around the metal center, it finds new interaction partners in the metal lone-pairs that can serve as hyperconjugative donors in the *3c,4e*-interactions. However, differences *between* the three metals are considerable, as one would expect from the different charge and size of Cu, Ag, and Au.

We can now discuss how different the observed behavior of the M···H–CH_3 complexes is in comparison to the conventional X···H-C hydrogen bonds where X is an electronegative heteroatom. Remarkably, although both types of supramolecular contacts lead to C–H elongation and a net donation of the metal or X into the σ^*_{CH}, the underlying electronic perturbations are dramatically different, in a few cases, even opposite! The most striking difference is related to the charges of C and H: the polarization (estimated from the square of contributing orbital coefficients in the C–H NBOs) of the C–H bond increases on H when M gets closer, while it is decreasing in classical X···H–C H-bonds when X approaches H. From the electronic point of view, this unusual nature of the electrostatic component in the M···H–CH_3 complexes renders them the opposite of the classic H-bonds. On the other hand, the covalent (*i.e.*, hyperconjugative, or charge-transfer) component of H-bonding is qualitatively similar for the two types of supramolecular interactions. Anti-electrostatic H-bonds (Scheme 5) have been defined for an H-bond between two ions of like-charge,[53] here we have an H-bond between two atoms of like partial charge, we propose to call this interaction "contra-electrostatic" H-bond.

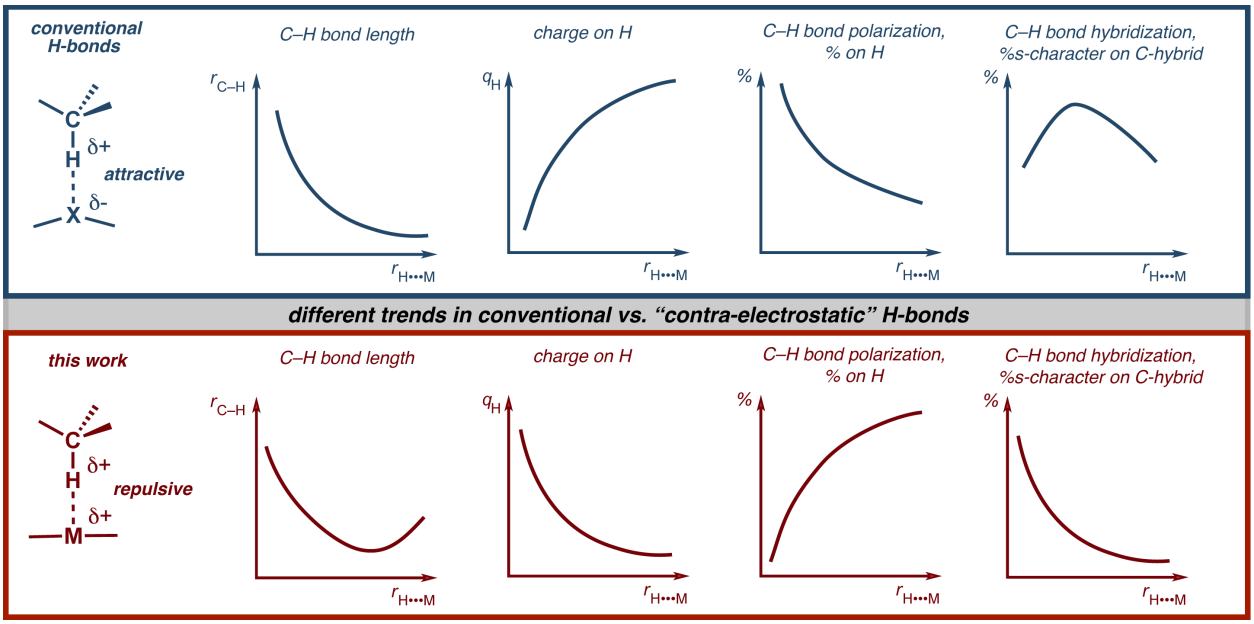

Scheme 5. Schematic representation of different trends in conventional H-bonds and "contra-electrostatic" H-bonds presented in this work.

We employed Natural Energy Decomposition Analysis (NEDA)[54-57] as an additional tool for analyzing the nature of the "contra-electrostatic" H-bonds in this study. Scheme 6a illustrates the total energy of M···H interactions along with the NEDA decomposition into three terms (electrical, charge transfer, and repulsion) for the three CH_4···M-NHC systems (with M = Au, Ag, and Cu). The electrostatic (electrical) term is further decomposed into its parts (static, induced polarization, and self-energy correction in Scheme 6b). For comparison, we also include the NEDA data for a conventionally H-bonded H_3C–H···NH_3 complex.

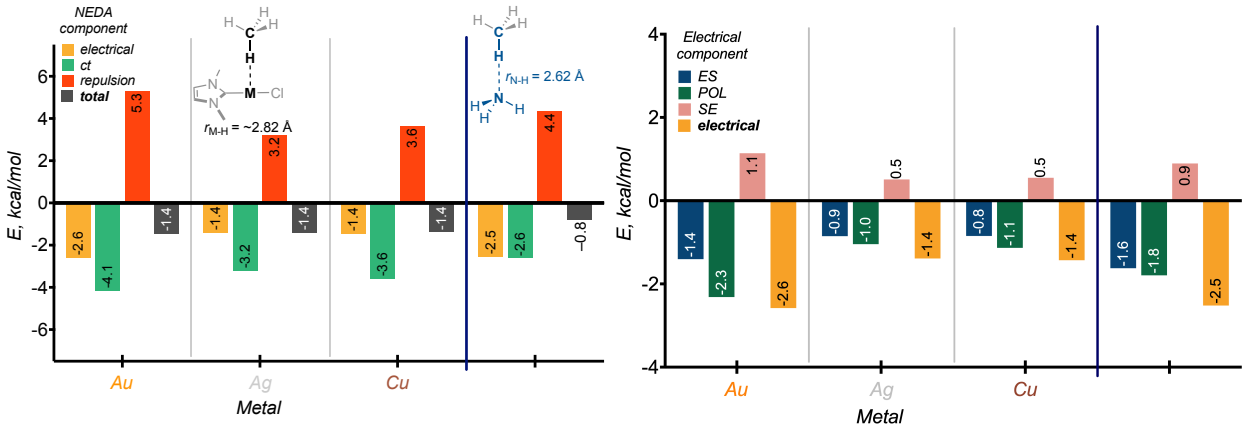

Scheme 6. Natural Energy Decomposition Analyses (NEDA) of CH_4···M–NHC systems (with M = Au, Ag, and Cu), and for H_3C–H···NH_3 complex as a conventional H-bond system. Left: The three components of NEDA (electrical, charge-transfer (*ct* above), and repulsion) are shown individually as well as the total interaction energy. Right: The electrostatic (electrical) term is further decomposed into its parts (static (*ES* above), induced polarization (*POL* above), and self-energy (*SE* above) correction).

Fortuitously, the total interaction energies for the three CH_4···M-NHC systems are nearly the same (–1.4 kcal/mol). The numbers are slightly negative, indicating that the "contra-electrostatic H-bonds" are attractive when optimization is conducted without any restraints. Each of these complexes is slightly stronger than the CH_4···NH_3 complex. When considering these differences, it is essential to remember that these interaction energies are *global,* originating from the multiple contacts between methane and different parts of the NHC–metal complex.
However, a comparison of individual contributions to the total interaction energies does reveal an interesting difference between the three CH_4···M-NHC systems and the CH_4···NH_3 complex. For the "contra-electrostatic complexes," the contribution of the charge transfer term (originating from hyperconjugative orbital interactions) is more significant than electrostatic stabilization whereas, for the CH_4···NH_3 complex, the contributions of electrostatic and charge-transfer (hyperconjugative) interactions are nearly the same.
The stabilizing electrostatic interactions are considerably decreased in the Cu and Ag complexes. Again, the Au-systems is different: both the overall stabilization and the overall destabilization are larger for the Au system than for the Ag and Cu systems, possibly due to Au's relativistic effects.

The difference in the electrical term can be further broken down into three components, as described in Eq. (1):

$$EL\ (Electrical) = ES\ (Static) + POL\ (Polarization) + SE\ (Self\ Energy\ correction) \qquad (1)$$

From the latter dissection, one can conclude that the difference in the Au system mostly originates from induced polarization dominating the electrical term (Scheme 6b). From that perspective, the higher polarizability of Au makes its complexes less "contra-electrostatic" than the Ag and Cu complexes.

Insights into the experimental observations – computational analysis of the full system:
Using the abovementioned insights, we can decipher the type of interactions revealed by the experimental data for the cyclodextrin-encapsulated metal complexes. Selected calculated ^{1}H NMR chemical shifts are given below for (α-ICyD^{Me})AgCl, (α-ICyD^{Me})CuCl, and (α-ICyD^{Me})AuCl complexes. The absolute values of the NMR shifts are well in line with the experimental ones (Table 1) for $H^{5(A,D)}$ and overestimated by ~0.6 ppm for $H^{5(C,F)}$, so the relative trend is well reproduced. The particular experimental behavior of the AuCl complex is also apparent in the computations (Figure 13).

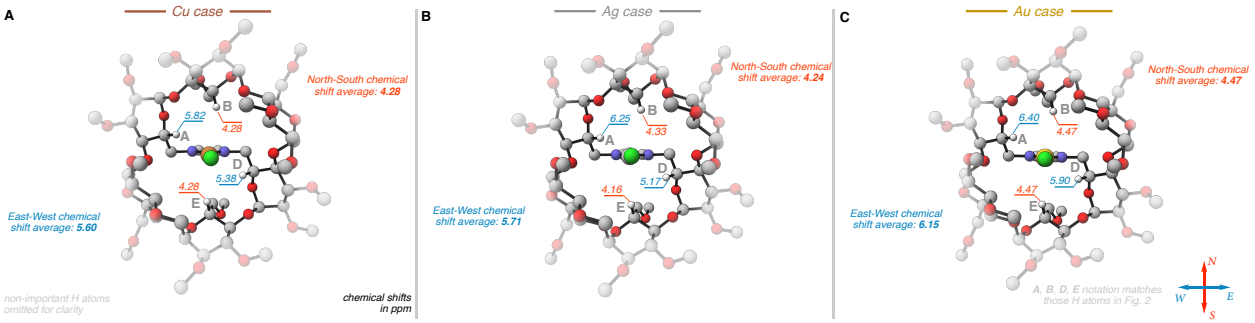

Figure 13. Selected calculated chemical shifts of (α-ICyD^{Me})AgCl, (α-ICyD^{Me})CuCl, and (α-ICyD^{Me})AuCl.

Computational dissection of key electronic parameters for the C–H bonds in the vicinity of the metal center in the experimentally studied cyclodextrin complexes is reported below. From the inspection of C–H bond length dependence from the M···H distance, it is clear that proximity to the metals leads to, at best, only a very slight elongation (Figure 14). Furthermore, this weak effect can be masked by other factors that affect by C–H bond length, *e.g.*, intramolecular stereoelectronic effects such as the anomeric or the gauche effects. The relatively small effects are consistent with our computational data for the model systems described above and contrast the relatively large effects that metals proximity has on the NMR chemical shifts (Figure 13). NBO analysis of the stereoelectronic interactions that may be responsible for the observed NMR trends was performed for the crystal structure geometries in the active centers of the Cu, Ag, and Au-systems (Figure 14). This analysis illustrates the presence of multiple donor-acceptor orbital interactions with different geometric parameters and significant variations in the H···M distances and the angles of approach. Due to the geometric differences, the interactions are not identical from the electronic viewpoint.

Interestingly, the contacts with the most deshielded H$^{5(A,D)}$ protons correspond to the largest donations from the metal lone-pairs to the σ^*_{CH} orbital. Encouragingly, the unusual effect of H···M distances on charges is well-reproduced in this experimental system. Indeed, H$^{5(A,D)}$ have lower charges than H$^{5(B,E)}$ because they are closer to the metal center. Conversely, the C$^{5(A,\ D)}$ atoms bear a greater positive charge than the C$^{5(B,E)}$. Hence, the combination of available experimental and computational data confirms that metal encapsulation inside the cyclodextrin cavity forces the C–H bond to point toward the metal, and reveal the attractive contra-electrostatic H-bonding.

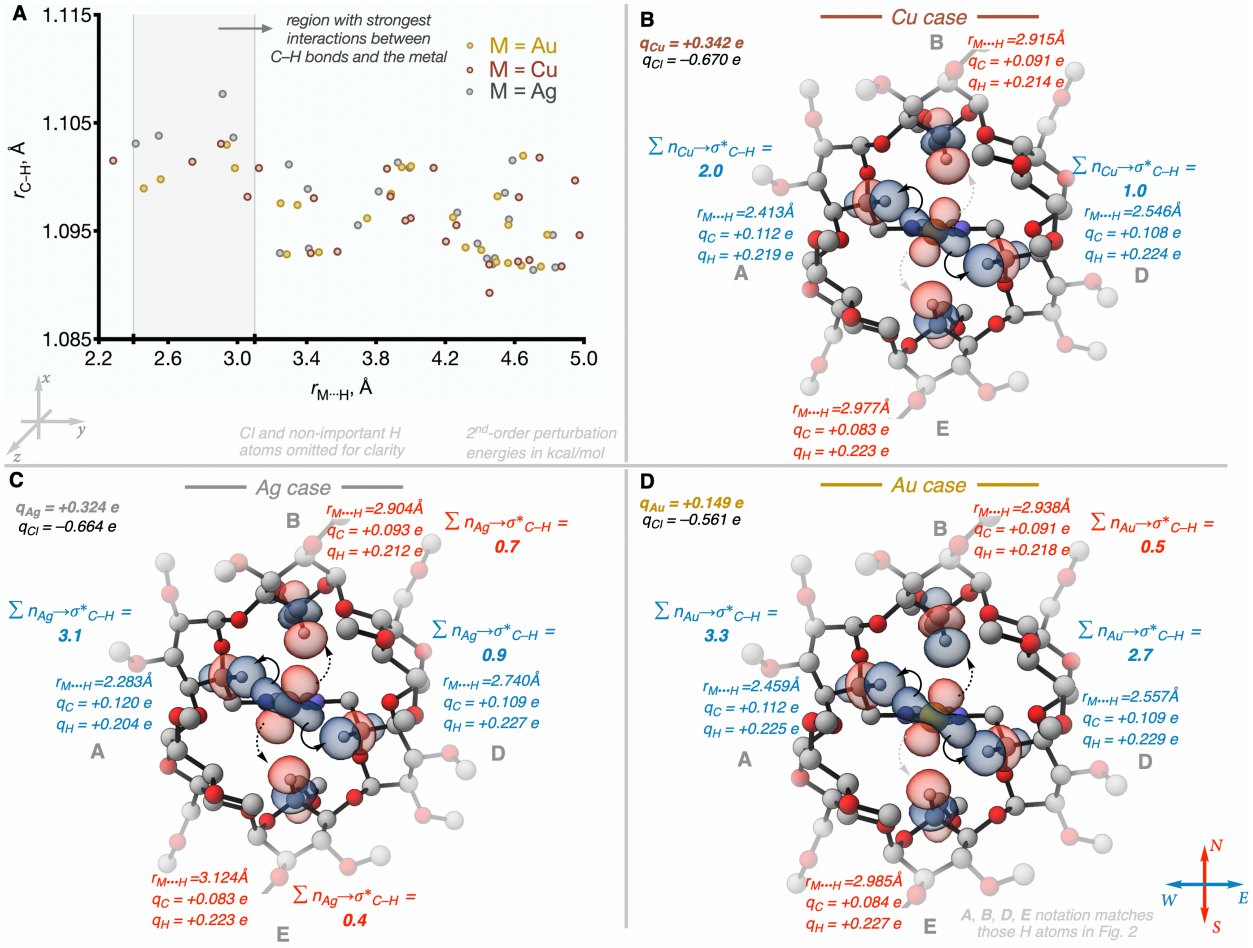

Figure 14. Computational analyses of full systems with Cu, Ag, and Au. The Cl atom and non-important H atoms were omitted for clarity in the picture. Only NBO interactions above the 0.05 kcal/mol threshold were included. **A**. Comparison of M···H distances *vs.* C–H distances, with a focus on the region where the metal interacts with most C–H bonds (for $r_{M\cdots H}$ between 2.4 and 3.1 Å), suggests a very weak C–H bond elongation. **B**. NBO and natural charge analyses for interactions between C–H within the region of interest and the Cu atom. No orbital donations from the metal to the C–H$^{5(B,E)}$ bonds. **C**. NBO and natural charge analyses for interactions between C–H within the region of interest and the Ag atom. Strongest donation from the metal center to the C–H^{5A} bond. **D**. NBO and natural charge analyses for interactions between C–H within the region of interest and the Au atom. No orbital donations from the metal to the C–H^{5E} bond, strong interactions in the C–H^{5A,} and C–H^{5D} bonds.

Finally, we have also performed the NEDA analysis on truncated systems that include the metal centers and the four closely located sugar moieties derived from the experimental data on the cyclodextrin cavity. Interestingly, the overall interaction energies were found to be attractive for each of the four contacts between the metal and the sugars (decoded as West, North, East, and South in Figure 15). The range of interaction energies for the twelve evaluated contacts varied considerably – from –1.4 to –6.5 kcal/mol.

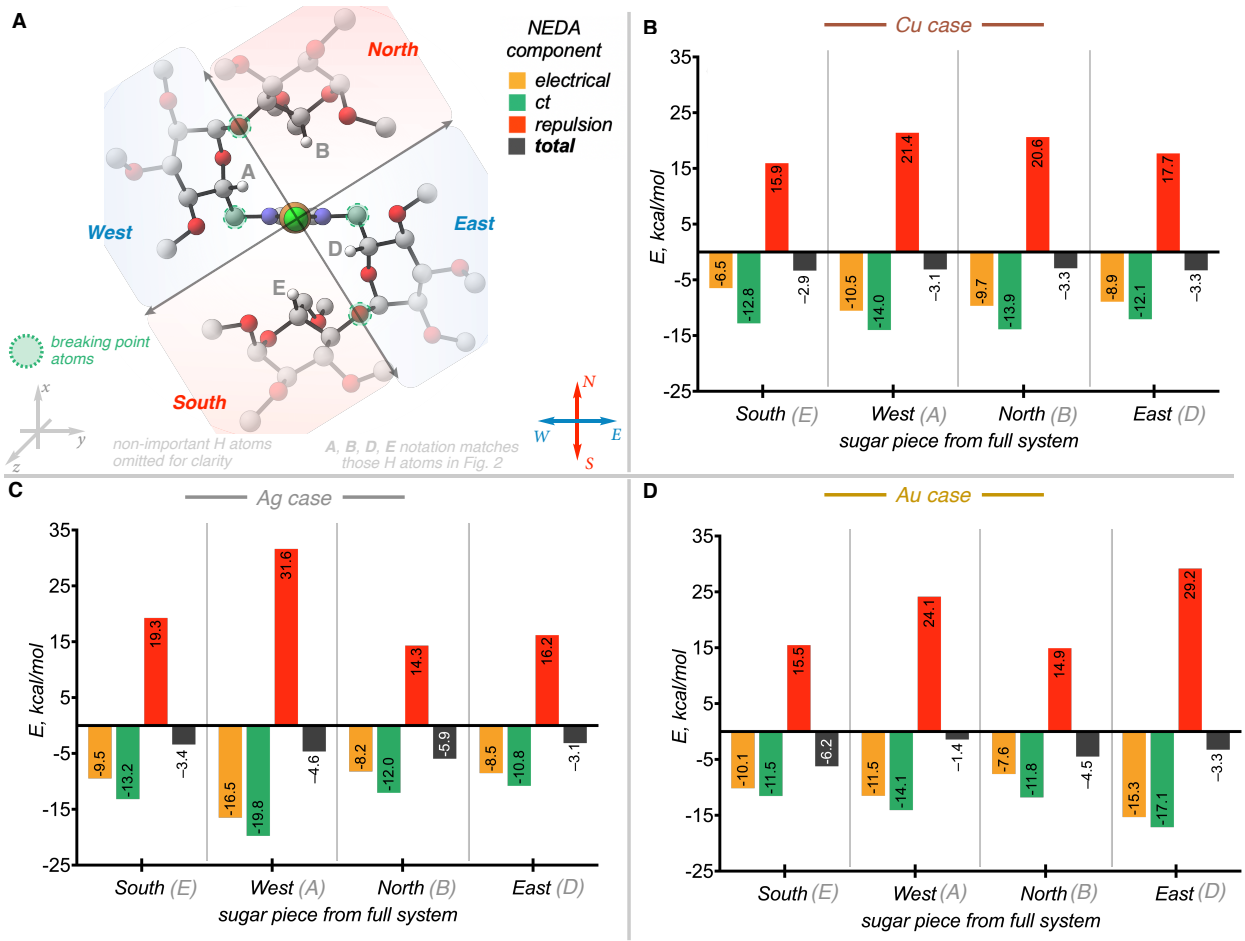

Figure 15. NEDA of trimmed full systems with Cu, Ag, and Au and their respective sugar pieces. Non-important H atoms were omitted for clarity. The three components of NEDA (electrostatic, charge-transfer, and repulsion) are shown individually as well as the total interaction energy. **A**. Trimmed full system with four sugars A, B, D, and E. For NEDA analyses on each quadrant contained the pair Cl-M-NHC (fragment 1) and its sugar (fragment 2); the other two sugars (C and F) were removed. **B**. NEDA analyses for interactions between each sugar within the region of interest and the Cl-Cu-NHC center. **C**. NEDA analyses for interactions between each sugar within the region of interest and the Cl-Ag-NHC center. **D**. NEDA analyses for interactions between each sugar within the region of interest and the Cl-Au-NHC center.

Remarkably, the greatest anisotropy of the interaction energies of the four sugar partners with the same metal center was found in the Au-system (–1.4 (West) *vs.* –6.2 (South) kcal/mol). In contrast, all four interactions were nearly identical for the Cu-system (–2.9 vs. –3.3 kcal/mol). The Au- and Ag-systems also show a more considerable variation in the relative magnitude of the individual repulsive and attractive (electrostatic, charge transfer = hyperconjugative) interactions than the Cu-system. Although the NEDA data are cumulative and reflect the interplay of multiple interactions, these data again illustrate the large variations in the nature of supramolecular interactions in these three systems.

Conclusion

Intrigued by the initial observation of unusual “anagostic” interaction between coinage metal complexes and introverted cavity protons of an NHC–capped cyclodextrin, we

explored these interactions theoretically. Our computations reveal that when a C–H bond is forced to interact with unpaired electron pairs at a positively charged metal, the covalent and electrostatic components of H-bonding do not work together as they do in classic H-bonds. We consider such interactions as "contra-electrostatic" H-bonds, as they combine the familiar orbital interaction pattern of conventional H-bonding with an unusual contra-electrostatic component. Whereas the Coulombic attraction is strongly stabilizing in the conventional C–H···X bonds where X is an electronegative main group element, electrostatics is destabilizing/repulsive in the C–H···M contacts when M is Au(I), Ag(I), or Cu(I) of NHC–M-Cl systems. In larger systems, this destabilization can be masked by the combination of the secondary effects between the other parts of the two interacting partners, including weaker electrostatics and dispersion interactions.

Crystal structures of NHC–capped *O*-methylated cyclodextrin metal complexes (α-ICyD^{Me})MCl (M=Ag, Cu, Au) allowed an experimental study of such intriguing C–H···M contacts inside the cavities. Together with the ^{1}H NMR data and the computational analysis, this data illustrates the unusual properties of the Au-complex. Unlike the Cu and Ag systems, the greater polarizability of Au can alleviate the lower contribution of electrostatic stabilization in such "contra-electrostatic" H-bonded complexes. In an attempt to generalize this weak interaction to other systems, we ran a CSD search looking for similar structural features ($d_{M–H}$ <2.6 Å and 130°<C–H–M angle<180°) and found around a 100 hits. Among them, we could identify one structure studied by Glorius that presented similar NMR and X-ray features,[58] making us believe that a contra-electrostatic H-bond was at play in that case too.

Considering the reactivity of these complexes as Lewis acids,[33-37] the recent work by Gabbaï showing that a positive charge in the proximity of Au atom could influence its reactivity[59] and the involvement of intra-cavity protons in stabilizing some transition states,[37] we hope that the correlations of NMR data and structural features of C–H···M interactions will help one to understand how a catalytic cavity is shaped for many different combinations of metal and ligands. Such understanding can facilitate the future design of highly selective metal-catalyzed reactions in confined spaces.

Computational details

We employed the B3LYP functional (with an ultrafine integration grid of 99,590 points) for all calculations. We used the following basis set scheme (BS1): H, C, N, O and Cl (6-311++G**); and Au/Ag/Cu (Def2-TVZPP, with Effective Core Potential).[60] Grimme's D3 version (with Becke and Johnson's damping) for empirical dispersion[61] corrections were also included. X-ray structures were refined by the optimization of hydrogen atoms, first with GFN2-xTB, and then reoptimized with B3LYP(D3BJ)/BS1 and an ultrafine integration grid.

Natural Bond Orbital[62-66] analyses (with *NBO6*[67] program) were performed in order to correlate orbital interactions at the metal center with the chemical shifts of protons and the lengths of participating C–H bonds. Additionally, NBO analyses for the full systems were performed at the B3LYP(D3BJ)/LanL2DZ with an ultrafine integration grid. To guarantee that our analysis solely corresponds to the explored variable, we have used several geometric constraints for the scans. For example, in the H_3C–H···metal distance

scans, we constrained other angles and dihedrals (*i.e.*, the C–H–M angle and the H–M–C1–N dihedral) that could influence the outcome, as described in the main text.

NBO analysis transforms the canonical delocalized molecular orbitals from DFT calculations into localized orbitals that are closely tied to the chemical bonding concepts. Each of the localized NBO sets is complete and orthonormal. The filled NBOs describe the hypothetical, strictly localized Lewis structure. The interactions between filled and antibonding orbitals represent the deviation from the Lewis structure and can be used to measure delocalization. For example, delocalizing interaction can be treated via the 2nd order perturbation energy approach as $E(2) = n_i \left|F_{ij}\right|^2 / \Delta E$, where n_i is the population of a donor orbital, F_{ij} is the Fock matrix element for the interacting orbitals i and j, and ΔE is the energy gap between these orbitals.

Natural Energy Decomposition Analysis (NEDA) calculations were performed (at the B3LYP(D3BJ)/LanL2DZ/(int=ultrafine) level of theory) on both $H_3C–H\cdots M–NHC$ and $H_3C–H\cdots NH_3$ systems, and on the truncated pieces of full systems where only one sugar interacts with the Cl–M–NHC system. This type of analysis proved useful when interrogating the system for different types of interactions between the sugar pieces of cyclodextrins and the metal centers.

NEDA is an energy partitioning procedure for molecular interactions.[68] Electrical interaction (EL), charge transfer (CT), and core repulsion (CORE) contributions are evaluated for self-consistent field (SCF) wavefunctions.[69] The total interaction energy is then given by $E = EL + CT + CORE$, in kcal/mol.

NMR shielding tensors were computed with the Gauge-Independent Atomic Orbital (GIAO) method,[70] at the (SMD[71]=$CHCl_3$)/B3LYP(D3BJ)/LanL2DZ/(int=ultrafine) level of theory. ^1H chemical shifts were taken with respect to the usual reference of TMS at the (NMR=GIAO) B3LYP/6-311+G(2d,p) level of theory.

All DFT and NBO6 calculations were performed with the *Gaussian 09 rev. D01* software package.[72] GFN2-xTB calculations were performed with Grimme's *xtb* (version 6.1).[73] NEDA calculations were performed with *NBO7*[74] linked to *Gaussian 16 rev. C01*.[75] Three-dimensional structures and orbital plots were produced with *CYLView* 1.0.1,[76] *IQmol* 2.8.0,[77] *Chemcraft* 1.8,[78] and *UCSF Chimera*.[79]

Supporting Information

Experimental and additional computational details reported in this work are available in the SI. The geometries and other relevant files for this work can be freely obtained at https://github.com/gabegomes/anagostic_contra-electrostatic_H-bonds. This material is available free of charge via the Internet at http://pubs.acs.org.

Acknowledgments

I.V.A and G. P. G. are grateful for the support of the National Science Foundation (Grant CHE-1800329). G. P. G gratefully acknowledges Canada's Natural Sciences and Engineering Research Council (NSERC) for the Banting Postdoctoral Fellowship. Part of computational resources was provided by NSF XSEDE (TG-CHE160006), and FSU Research Computing Center. G. P. G. thanks Professor Alán Aspuru-Guzik (University of Toronto, Vector Institute for Artificial Intelligence) for the support and Compute

Canada for computational resources. NEDA computations were performed on the *niagara* supercomputer at the SciNet HPC Consortium. SciNet is funded by: the Canada Foundation for Innovation; the Government of Ontario; Ontario Research Fund - Research Excellence; and the University of Toronto. X.L. and G.X. thank the CSC for a PhD grant. P.B.A, S.R., M.S. thank the LabEx MiChem part of French state funds managed by the ANR within the Investissements d'Avenir programme under reference ANR-11-IDEX-0004-02, and Cyclolab (Hungary) for a generous supply of α-cyclodextrin. We thank Dr. Robert Pollice and Dr. Kjell Jorner (University of Toronto) for valuable discussions. The first version of this manuscript has been posted as a preprint on *ChemRxiv*.[80]

References and Notes

[1] L. Brammer, *Dalton Trans*. **2003**, 3145-3157.

[2] J. Zhao, A. S. Goldman, J. F. Hartwig, *Science* **2005**, *307*, 1080-1082.

[3] J. C. Lewis, J. Wu, R. G. Bergman, J. A. Ellman, *Organometallics* **2005**, *24*, 5737-5746.

[4] C. Hall, R. N. Perutz, *Chem. Rev*. **1996**, *96*, 3125-3146.

[5] S. Trofimenko*, J. Am. Chem. Soc*. **1970**, *9*, 2493-2499.

[6] M. Brookhart, M. L. H. Green, *J. Organomet. Chem*. **1983**, *250*, 395-408.

[7] R. H. Crabtree, *Chem. Rev*. **1995**, *95*, 987-1007.

[8] R. H. Crabtree, *Angew. Chem. Int. Ed. Engl*. **1993**, *32*, 789-805.

[9] A. H. Janowicz, R. G. Bergman, *J. Am. Chem. Soc*. **1982**, *104*, 352-354.

[10] R. A. Periana, R. G. Bergman, *J. Am. Chem. Soc*. **1986**, *108*, 7332-7346.

[11] R. M. Bullock, C. E. L. Headford, S. E. Kegley, J. R. Norton, *J. Am. Chem. Soc*. **1985**, *107*, 727-729.

[12] G. L. Gould, D. M. Heinekey, *J. Am. Chem. Soc*. **1989**, *111*, 5502-5504.

[13] H. Chen, S. Schelecht, T. C. Semple, J. F. Hartwig, *Science* **2000**, *287*, 1995-1997.

[14] W. I. Sundquist, D. P. Bancroft, S. J. Lippard, *J. Am. Chem. Soc*. **1990**, *112*, 1590-1596.

[15] Y. Wenbin, O. Eisenstein, R. H. Crabtree, *Inorg. Chim. Acta* **1997**, *254*, 105-111.

[16] E. S. Shubina, A. N. Krylov, A. Z, Kreindlin, M. I. Rybinskaya, L. M. Epstein, *J. Mol. Struct*. **1994**, *465*, 259-262.

[17] M. P. Mitoraj, M. G. Babashkina, K. Robeyns, F. Sagan, D. W. Szczepanik, Y. V. Seredina, Y. Garcia, D. A. Safin, *Organometallics* **2019**, *38*, 1973-1981.

[18]Y. Zhang, J. C. Lewis, R. G. Bergman, J. A. Ellman, E. Oldfield, *Organometallics* **2006**, *25*, 3515-3519.

[19] M. Brookhart, M. L. H. Green, G. Parkin, *Proc. Natl. Acad. Sci. USA* **2007**, *104*, 6908-6914.

[20] W. Scherer, A. C. Dunbar, J. E. Barquera-Lozada, D. Schmitz, G. Eickerling, D. Kratzert, D. Stalke, A. Lanza, P. Macchi, N. P. M. Casati, J. Ebad-Allah, C. Kuntscher, *Angew. Chem. Int. Ed*. **2015**, *54*, 2505-2509.

[21] D. Braga, F. Grepioni, E. Tedesco, K. Biradha, G. R. Desiraju, *Organometallics* **1997**, *16*, 1846-1856.

[22] E. S. Smirnova, F. Acuña-Parés, E. C. Escudero-Adán, C. Jelsch, J. Lloret-Fillol, *Eur. J. Inorg. Chem*. **2018**, *2018*, 2612-2620.

[23] H. Schmidbaur, H. G. Raubenheimer, L. Dobrzanska, *Chem. Soc. Rev*. **2014**, *43*, 345-380.

[24] F. Kraus, H. Schmidbaur, S.S. Al-juaid, *Inorg. Chem.* **2013**, *52*, 9669-9674.

[25] L.-A. Schaper, X. Wei, S. J. Hock, A. Pöthig, K. Öfele, M. Cokoja, W. A. Herrmann, F. E. Kühn, *Organometallics* **2013**, *32*, 3376-3384.

[26] L. Koskinen, S. Jääskeläinen, E. Kalenius, P. Hirva, M. Haukka, *Cryst. Growth Des*. **2014**, *14*, 1989-1997.

[27] M. A. Bakar, M. Sugiuchi, M. Iwasaki, Y. Shichibu, K. Konishi, *Nat. Commun*. **2017**, *8*, 576.

[24] a) H. Schmidbaur, H. G. Raubenheimer, L. Dobrzanska, *Chem. Soc. Rev*. **2014**, *43*, 345-380; b) F. Kraus, H. Schmidbaur, S.S. Al-juaid, *Inorg. Chem.* **2013**, *52*, 9669-9674.

[25] L.-A. Schaper, X. Wei, S. J. Hock, A. Pöthig, K. Öfele, M. Cokoja, W. A. Herrmann, F. E. Kühn, *Organometallics* **2013**, *32*, 3376-3384.

[26] L. Koskinen, S. Jääskeläinen, E. Kalenius, P. Hirva, M. Haukka, *Cryst. Growth Des*. **2014**, *14*, 1989-1997.

[27] M. A. Bakar, M. Sugiuchi, M. Iwasaki, Y. Shichibu, K. Konishi, *Nat. Commun*. **2017**, *8*, 576.

[28] a) M. Rigoulet, S. Massou, E. D. Sosa Carrizo, S. Mallet-Ladeira, A. Amgoune, K. Miqueu, D. Bourissou, *Proc. Natl. Acad. Sci. USA*, 2019, **116**, 46-51; b) M. Straka, E. Andris, J. Vícha, A. Růžička, J. Roithová, L. Rulíšek, *Angew. Chem. Int. Ed*. **2019**, *58*, 2011-2016.

[29] M. Kumar, J. S. Francisco, *J. Am. Chem. Soc*. **2020**, *142*, 6001-6006.

[30] J. R. Krumper, M. Gerisch, A. Magistrato, U. Rothlisberger, R. G. Bergman, T. D. Tilley, *J. Am. Chem. Soc*. **2004**, *126*, 12492-12502.

[31] M. Stepien, L. Latos-Grazynski, L. Szterenberg, J. Panek, Z. Latajka, *J. Am. Chem. Soc*. **2004**, *126*, 4566-4580.

[32] S. G. Kazarian, P. A. Hamley, M. Poliakoff, *J. Am. Chem. Soc*. **1993**, *115*, 9069-9079.

[33] M. Guitet, P. Zhang, F. Marcelo, Tugny, J. Jiménez-Barbero, O. Buriez, C. Amatore, V. Mouriès-Mansuy, J.-P. Goddard, L. Fensterbank, Y. Zhang, S. Roland, M. Ménand, M. Sollogoub, *Angew. Chem. Int. Ed*. **2013**, *52*, 7213-7218.

[34] a) P. Zhang, C. Tugny, J. Meijide Suárez, M. Guitet, E. Derat, N. Vanthuyne, Y. Zhang, O. Bistri, V. Mouriès-Mansuy, M. Ménand, S. Roland, L. Fensterbank, M. Sollogoub, *Chem* **2017**, *3*, 174-191; b) C. Tugny, N. del Rio, M. Koohgard, N. Vanthuyne, D. Lesage, K. Bijouard, P. Zhang, J. Meijide Suárez, S. Roland, O. Bistri-Aslanoff, M. Sollogoub, L. Fensterbank, V. Mouriès-Mansuy, *ACS Catal.* **2020**, *10*, 5964-5972.

[35] P. Zhang, J. Meijide Suárez, T. Driant, E. Derat, Y. Zhang, M. Ménand, S. Roland, M. Sollogoub, *Angew. Chem. Int. Ed.* **2017**, *56*, 10821-10825.

[36] Z. Wen, Y. Zhang, S. Roland, M. Sollogoub, *Eur. J. Org. Chem.* **2019**, 2682-2687.

[37] G. Xu, S. Leloux, P. Zhang, J. Meijide Suárez, Y. Zhang, E. Derat, M. Ménand, O. Bistri-Aslanoff, S. Roland, T. Leyssens, O. Riant, M. Sollogoub, *Angew. Chem. Int. Ed.* **2020**, *59*, 7591-7597.

[38] For a comprehensive overview of how confined spaces can impact chemical reactivity, check: a) A. B. Grommet, M. Feller, R. Klajn, *Nat. Nanotechnol*. **2020**, *15*, 256-271; b) S. Roland, J. Meijide Suarez, M. Sollogoub, *Chem. Eur. J.* **2018**, *24*, 12464-12473.

[39] X. Zhu, G. Xu, L.-M. Chamoreau, Y. Zhang, V. Mansuy, L. Fensterbank, O.Bistri-Aslanoff, S. Roland, M. Sollogoub, *Chem. Eur. J.* **2020**, *26*, 15901-15909.

[40] I. V. Alabugin, S. Bresch, G. P. Gomes, *J. Phys. Org. Chem*. **2015**, *28*, 147-162.

[41] I. V. Alabugin, M. Manoharan, *J. Comp. Chem*. **2007**, *28*, 373-390.

[42] I. V. Alabugin, M. Manoharan, S. Peabody, F. Weinhold, *J. Am. Chem. Soc*. **2003**, *125*, 5973-5987.

[43] Homogenous Gold Catalysis. Eds. V. Michelet, F. D. Toste, Imperial College Press London. 2014.

[44] Modern Gold Catalysis Synthesis. Eds. A. S. K. Hashmi, F. D. Toste, John Wiley & Sons. 2012.

[45] L. Fensterbank, M. Malacria, *Acc. Chem. Res*. **2014**, *47*, 953-965.

[46] R. Dorel, A. M. Echavarren, *Chem. Rev*. **2015**, *115*, 9028-9072.

[47] P. W. Peterson, R. K. Mohamed, I. V. Alabugin, *Eur. J. Org. Chem*. **2013**, *2013*, 2505-2527.

[48] G. P. Gomes, I. V. Alabugin, *J. Am. Chem. Soc*. **2017**, *139*, 3406-3416.

[49] D. Vidhani, M. Krafft, I. V. Alabugin, *J. Am. Chem. Soc*. **2016**, *138*, 2769-2779.

[50] K. Pati, G. P. Gomes, T. Harris, I. V. Alabugin, *Org. Lett*. **2016**, *18*, 928-931.

[51] K. Pati, I. V. Alabugin, *Eur. J. Org. Chem*. **2014**, *19*, 3986-3990.

[52] D. V. Vidhani, J. W. Cran, M. E. Krafft, M. Manoharan, I. V. Alabugin, *J. Org. Chem*. **2013**, *78*, 2059-2073.

[53] F. Weinhold, R. A. Klein, *Angew. Chem. Int. Ed*. **2014**, *53*, 11214-11217.

[54] E. D. Glendening, A. Streitwieser, *J. Chem. Phys*. **1994**, *100*, 2900-2909.

[55] E. D. Glendening, *J. Am. Chem. Soc*. **1996**, *18*, 2473-2482.

[56] G. K. Schenter, E. D. Glendening, *J. Phys. Chem*. **1996**, *100*, 17152-17156.

[57] E. D. Glendening, *J. Phys. Chem. A* **2005**, *109*, 11936-11940.

[58] C. Lohre, C. Nimphius, M. Steinmetz, S. Würtz, R. Fröhlich, C. G. Daniliuc, S. Grimme, F. Glorius, *Tetrahedron* **2012**, *68* 7636-7644.

[59] a) L. C. Wilkins, Y. Kim, E. D. Litle, F. P. Gabbaï, *Angew. Chem. Int. Ed.* **2019**, *58*, 18266-18270; b) E. D. Litle, L. C. Wilkins, F. P. Gabbaï, *Chem. Sci.* **2021**, DOI: 10.1039/D0SC05777K

[60] Basis sets for Au, Ag, Cu were obtained from the Basis Set Exchange (https://www.basissetexchange.org).

[61] S. Grimme, J. Antony, S. Ehrlich, H. Krieg, *J. Chem. Phys*. **2010**, *132*, 154104.

[62] F. Weinhold, C. R. Landis, E. D. Glendening, *Int. Rev. Phys. Chem*. **2016**, *35*, 399-440.

[63] A. E. Reed, F. Weinhold, *Chem. Phys*.**1985**, 83, 1736-1740.

[64] A. E. Reed, F. Weinhold, *Isr. J. Chem*. **1991**, *31*, 277-285.

[65] A. E. Reed, L. A. Curtiss, F. Weinhold, *Chem. Rev*. **1988**, *88*, 899-926.

[66] F. Weinhold, P. v. R. Schleyer, *Encyclopedia of Computational Chemistry*: John Wiley & Sons, Inc. New-York, 1998, **3**, 1792.

[67] *NBO 6.0. Program*: E. D. Glendening, J. K. Badenhoop, A. E. Reed, J. E. Carpenter, J. A. Bohmann, C. M. Morales, C. R. Landis, F. Weinhold, Theoretical Chemistry Institute, University of Wisconsin, Madison, 2013.

[68] A key element of the NEDA approach is the evaluation of "perturbed" fragment wavefunctions, Ψ_A^{def}, one for each of the fragments that comprise the molecular complex. These wavefunctions are constructed from the eigenvectors of local fragment blocks of the Fock or Kohn-Sham matrix expressed in the NAO, NBO, or NLMO basis. Orthogonality of the basis orbitals ensures that the sets of eigenvectors for different fragments are mutually orthogonal. The charge distributions described by the perturbed wavefunctions arise from electric field quantum mechanical effects experienced by the fragments within the complex. A localized wavefunction, Ψ^{loc}, for the complex is then constructed as an antisymmetrized product of perturbed fragment wavefunctions. NEDA additionally employs the supermolecule wavefunction, Ψ, of the complex the SCF-converged wavefunctions of the isolated fragments, Ψ_A.

[69] Definitions according to the NEDA manual (https://nbo6.chem.wisc.edu/tut_neda.htm): "Electrical" (EL) component, considered to represent the classical-like Coulombic interactions between atomic charges, bond dipoles the like, "Steric exchange" (EX) component, considered to represent Pauli exchange-type repulsions between filled orbitals (or the quasi-classical "Lennard-Jones repulsion" between hard-shell sphere atoms), "Charge transfer" (CT) component, considered to represent resonance-type "delocalization" interactions between filled orbitals of one subunit unfilled orbitals of the other. The EL component may be further divided into static (ES) induced "polarization" (POL) components [with associated "self-energy" (SE) correction for the energetic penalty at each polarizing center], post-HF "correlation" (CORR) or other components may be added in more refined treatments.

[70] J. R. Cheeseman, G. W. Trucks, T. A. Keith, M. J. Frisch, *J. Chem. Phys*. **1996**, *104*, 5497-5509.

[71] A. V. Marenich, C. J. Cramer, D. G. Truhlar, *J. Phys. Chem. B* **2009**, *113*, 6378-6396.

[72] Gaussian '09: M. J. Frisch, G. W. Trucks, H. B. Schlegel, G. E. Scuseria, M. A. Robb, J. R. Cheeseman, G. Scalmani, V. Barone, B. Mennucci, G. A. Petersson, H. Nakatsuji, M. Caricato, X. Li, H. P. Hratchian, A. F. Izmaylov, J. Bloino, G. Zheng, J. L. Sonnenberg, M. Hada, M. Ehara, K. Toyota, R. Fukuda, J. Hasegawa, M. Ishida, T. Nakajima, Y. Honda, O. Kitao, H. Nakai, T. Vreven, J. A. Jr. Montgomery, J. E. Peralta, F. Ogliaro, M. Bearpark, J. J. Heyd, E. Brothers, K. N. Kudin, V. N. Staroverov, R. Kobayashi, J. Normand, K. Raghavachari, A. Rendell, J. C. Burant, S. S. Iyengar, J. Tomasi, M. Cossi, N. Rega, M. J. Millam, M. Klene, J. E. Knox, J. B. Cross, V. Bakken, C. Adamo, J. Jaramillo, R. Gomperts, R. E. Stratmann, O. Yazyev, A. J. Austin, R. Cammi, C. Pomelli, J. W. Ochterski, R. L. Martin, K. Morokuma, V. G. Zakrzewski, G. A. Voth, P. Salvador, J. J. Dannenberg, S. Dapprich, A. D. Daniels, Farkas, J. B. Foresman, J. V. Ortiz, J. Cioslowski, D. J. Fox, Gaussian, Inc. Wallingford CT, 2009.

[73] *xtb* can be freely obtained at**:** https://github.com/grimme-lab/xtb**s.** C. Bannwarth, S. Ehlert, S. Grimme, *J. Chem. Theory Comput*. **2019**, *15*, 1652-1671.

[74] *NBO 7.0* can be obtained at: http://nbo7.chem.wisc.edu. E. D. Glendening, C. R. Landis, F. Weinhold, *J. Comput. Chem*. **2019**, *40*, 2234-2241.

[75] Gaussian '16, Revision C.01, M. J. Frisch, G. W. Trucks, H. B. Schlegel, G. E. Scuseria, M. A. Robb, J. R. Cheeseman, G. Scalmani, V. Barone, G. A. Petersson, H. Nakatsuji, X. Li, M. Caricato, A. V. Marenich, J. Bloino, B. G. Janesko, R. Gomperts, B. Mennucci, H. P. Hratchian, J. V. Ortiz, A. F. Izmaylov, J. L. Sonnenberg, D. Williams-Young, F. Ding, F. Lipparini, F. Egidi, J. Goings, B. Peng, A. Petrone, T. Henderson, D. Ranasinghe, V. G. Zakrzewski, J. Gao, N. Rega, G. Zheng, W. Liang, M. Hada, M. Ehara, K. Toyota, R. Fukuda, J. Hasegawa, M. Ishida, T. Nakajima, Y. Honda, O. Kitao, H. Nakai, T. Vreven, K. Throssell, J. A. Jr. Montgomery, J. E. Peralta, F. Ogliaro, M. J. Bearpark, J. J. Heyd, E. N. Brothers, K. N. Kudin, V. N. Staroverov, T. A. Keith, R. Kobayashi, J. Normand, K. Raghavachari, A. P. Rendell, J. C. Burant, S. S. Iyengar, J. Tomasi, M. Cossi, J. M. Millam, M. Klene, C. Adamo, R. Cammi, J. W. Ochterski, R. L. Martin, K. Morokuma, O. Farkas, J. B. Foresman, D. J. Fox, Gaussian, Inc. Wallingford CT, 2016.

[76] CYLview, 1.0b, Legault, C. Y. Université de Sherbrooke, 2009 (http://www.cylview.org)

[77] IQmol 2.8.0, http://iqmol.org, accessed in March 2017

[78] *ChemCraft 1.8* http://www.chemcraftprog.com, accessed in February 2016.

[79] Some of the molecular graphics in this work were produced with UCSF Chimera, developed by the Resource for Biocomputing, Visualization, Informatics at the University of California, San Francisco, with support from NIH P41-GM103311. E. F. Pettersen, T. D. Goddard, C. C. Huang, G. S. Couch, D. M. Greenblatt, E. C. Meng, T. E. Ferrin, *J. Comput. Chem*. **2004**, *25*, 1605-1612.

[80] G. P. Gomes, G. Xu, X. Zhu, L.-M. Chamoreau, O. Bistri-Aslanoff, S. Roland, I. V. Alabugin, M. Sollogoub, "Mapping the coordination space for the C-H···M interactions in confined spaces: (α-ICyD^{Me})Au, Ag, Cu complexes reveal "contra-electrostatic H-bonds" masquerading as anagostic interactions", preprint on ChemRxiv doi: 10.26434/chemrxiv.12167916. 2020.